# NASA Technical Memorandum 84577



# CYCLIC DEBONDING OF ADHESIVELY BONDED COMPOSITES

S. Mall, W. S. Johnson, and R. A. Everett, Jr.

November 1982

National Aeronautics and Space Administration

Langley Research Center
Hampton, Virginia 23665

# CYCLIC DEBONDING OF ADHESIVELY BONDED COMPOSITES

S. Mall,* W. S. Johnson, and R. A. Everett, Jr.**

NASA Langley Research Center
Hampton, Virginia 23665

To analyze the fatigue behavior of a simple composite-to-composite bonded joint, a combined experimental and analytical study of the cracked-lap-shear specimen subjected to constant-amplitude cyclic loading was undertaken. Two bonded systems were studied: T300/5208*** graphite/epoxy adherends bonded with adhesives EC 3445*** and FM-300***. For each bonded system, two specimen geometries were tested: (1) a strap adherend of 16 plies bonded to a lap adherend of 8 plies, and (2) a strap adherend of 8 plies bonded to a lap adherend of 16 plies. In all specimens tested, the fatigue failure was in the form of cyclic debonding with some $0^{o}$ fiber pull-off from the strap adherend. The debond always grew in the region of adhesive that had the highest mode I (peel) loading and that region was close to the adhesive-strap interface. Furthermore, the measured cyclic debond growth rates correlated well with total strain energy release rates $G_T$ as well as with its components $G_I$ (peel) and $G_{II}$ (shear) for the mixed-mode loading in the present study.

---

*University of Maine, on leave of absence at NASA Langley Research Center.

**Structures Laboratory, U.S. Army Research and Technology Laboratories (AVRADCOM), NASA Langley Research Center.

***The use of trade names in this paper does not constitute endorsement, either expressed or implied, by the National Aeronautics and Space Administration.

## INTRODUCTION

To increase performance and fuel economy, aerospace industries have been turning more and more to the use of advanced composites in both commercial and military aircraft. These materials offer excellent strength-to-weight and stiffness-to-weight ratios. But their efficient application requires more sophisticated joining methods than used in metallic structures. Because composites are severely weakened by fastener holes, their weight advantage may be lessened when mechanically fastened joints are used. Adhesive bonding, on the other hand, provides a desirable alternative to mechanical fastening because of the following potential advantages: (1) higher joint efficiency index (relative strength/weight of the joint region), (2) lower part count, (3) no strength degradation of basic laminate due to fastener holes, (4) less expensive and simpler fabrication techniques, (5) lower maintenance costs, and (6) potential corrosion problems avoided.

Design methods for adhesively bonded composites require criteria to predict both strength and durability. Although analytical and experimental work has been reported on the static strength of bonded composites,[1-3] very little information is available on their fatigue behavior. Several possible fatigue failure modes exist for bonded composites: cyclic debonding (i.e., progressive separation of the adhesive bond under cyclic load), interlaminar damage (delamination), adherend fatigue, or a combination of these. Therefore, life predictions require a basic understanding of the mechanics associated with each failure mode.

Many of the results obtained in cyclic debonding studies of composite-to-metal joints[4] and metal-to-metal joints[5] may be applicable to the present case of composite-to-composite joints. In the study by Roderick et al.,[4] the fracture mechanics concept of strain energy release rate was used to model the cyclic failure of bonded composite-to-metal joints. This is similar to the approach in metals where fatigue-crack-propagation rate is correlated with the strain energy release rate. The total strain energy release rate, $G_T$, associated with the cyclic failure of an adhesive bond can be resolved into three components $G_I$, $G_{II}$, and $G_{III}$ associated with three debonding modes: I (opening), II (sliding), and III (tearing), respectively. However, in most practical applications, only $G_I$ and $G_{II}$, due to peel and shear stresses, respectively, exist near the debond front during cyclic loading. Using metal-to-metal joints, Brussat et al.[5] developed the cracked-lap-shear specimen to study the effect of mixed-mode ($G_I$ and $G_{II}$) loading on adhesive joints. Romanko[6] has extended these fracture mechanics concepts to investigate the failure of adhesive joints under various environmental conditions involving temperature, moisture, etc. Everett[7] recently showed that the strain energy release rate $G_I$

associated with peel stress had a significant effect on cyclic bonding.

The objective of the present study was to analyze the fatigue behavior of simple composite-to-composite bonded joints subjected to constant-amplitude cyclic loading. For this purpose, graphite/epoxy (T300/5208) cracked-lap-shear specimens were tested using EC 3445 and FM-300 adhesives. This investigation focused on the correlation of the measured cyclic debond rates with strain energy release rates calculated using a finite element analysis of the cracked-lap-shear specimen. Failure modes of this simple joint were also analyzed to investigate the relative influence of $G_I$ and $G_{II}$.

## NOMENCLATURE

| | |
|---|---|
| $a$ | length of debond, mm |
| $\frac{da}{dN}$ | debond growth rate, mm/cycle |
| $B$ | width of specimen, mm |
| $c,n$ | curve-fit parameters |
| $E$ | Young's modulus of adhesive, GPa |
| $E_1,E_2$ | Young's moduli of composite, GPa |
| $G$ | shear modulus of adhesive, GPa |
| $G_{12}$ | shear modulus of composite, GPa |
| $G_I$ | mode I strain energy release rate, $J/m^2$ |
| $G_{II}$ | mode II strain energy release rate, $J/m^2$ |
| $G_{III}$ | mode III strain energy release rate, $J/m^2$ |
| $G_T$ | total strain energy release rate ($= G_I + G_{II}$), $J/m^2$ |
| $N$ | number of cycles |
| $P$ | applied load, kN |
| $r$ | residual from least-square curve fit |
| $\nu$ | Poisson's ratio of adhesive |
| $\nu_{12},\nu_{23}$ | Poisson's ratios of composite |

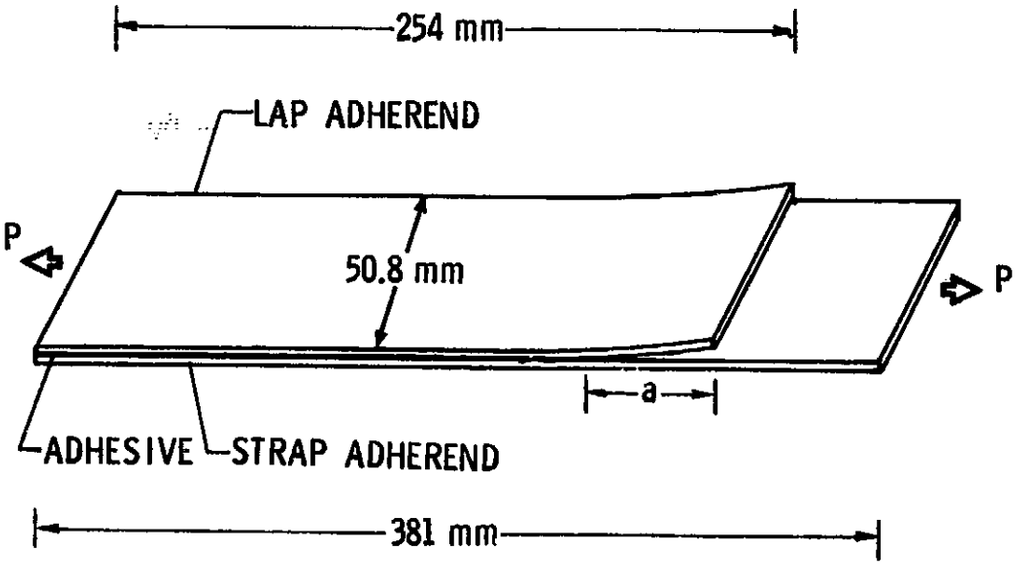


Figure 1. Cracked-lap-shear specimen.

## EXPERIMENTS

### Test Specimen

The cracked-lap-shear specimen, shown in Figure 1, was employed in the present study because it represents a simple structural joint subjected to in-plane loading. Both shear and peel stresses are present in the bond line of this joint. The magnitude of each component of this mixed-mode loading can be modified by changing the relative thicknesses of strap and lap adherends.[5,8] For the present study, the strap and lap adherends had 8 or 16 plies. These adherends had a quasi-isotropic layup and were typical of those currently employed in an Army program to build an all-composite helicopter airframe which is almost entirely adhesively bonded.[9]

Two bonded systems were studied—graphite/epoxy (T300/5208) adherends bonded with EC 3445 adhesive and with FM-300 adhesive. The EC 3445 adhesive is a thermosetting paste adhesive with a cure temperature of 121°C. Specimens with this adhesive were fabricated using conventional secondary bonding procedure. However, specimens with FM-300 adhesive were fabricated by a co-curing procedure whereby adherends were cured and bonded simultaneously. The FM-300 is a modified epoxy adhesive supported with a carrier cloth with a cure temperature of 177°C. These adhesives, as well as the concepts of

Table I. Adhesive Material Properties

| Adhesives | Modulus, GPa E | G | Poisson's Ratio ν |
|---|---|---|---|
| EC 3445 (3M Company) | 1.81 | 0.65 | 0.4 |
| FM-300 (American Cyanamid Company) | 2.32 | 0.83 | 0.4 |

secondary and co-cure bonding, are also being employed in the bonded all-composite helicopter airframe mentioned previously.[9] The bonding process followed the manufacturer's recommended procedures for each adhesive. The nominal adhesive thickness was 0.10 and 0.25 mm for the EC 3445 and FM-300, respectively.

The Young's modulus of FM-300 adhesive was calculated from the shear modulus provided by the manufacturer, assuming the adhesive to be an isotropic material. Poisson's ratio was assumed to be 0.4 for both adhesives which is a typical value for adhesives. The EC 3445 adhesive is the paste version of the AF-55 adhesive film. Therefore, the Young's modulus of EC 3445 was calculated from the shear modulus of AF-55,[10] assuming the adhesive to be an isotropic material. The material properties of both adhesives are given in Table I.

The composite adherends consisted of quasi-isotropic lay-ups of $[0^\circ/45^\circ/-45^\circ/90^\circ]_S$ and $[0^\circ/45^\circ/-45^\circ/90^\circ]_{2S}$. The material properties of graphite/epoxy, presented in Table II, were obtained from reference 11. For each bonded system, two types of specimen were tested: (1) thin lap adherend of 8 plies bonded to thick strap adherend of 16 plies, and (2) thick lap adherend of 16 plies bonded to thin strap adherend of 8 plies. This arrangement provided four sets of specimens. Initially, the lengths of strap and lap adherends were 381 and 254 mm, respectively (a total of 127 mm was for grip support on both ends). However, specimens with a thick co-cured lap adherend were modified due to a pinched-off edge obtained during fabrication. This pinched-off edge, as discussed in reference 12, caused a nonuniform thickness of lap adherend and adhesive near the end of the overlap. To avoid problems due to this nonuniform thickness, the pinched-off ends were removed by machining. In the resulting modified specimen, lengths of strap and lap adherends were 305 and 203 mm, respectively.

## Testing Procedure

All specimens were tested in a closed-loop hydraulic test machine at a frequency of 10 Hz. In all tests, constant amplitude

Table II. Graphite/Epoxy[a] Adherend Material Properties

| Modulus,[b] GPa | | | Poisson's Ratio[b] | |
|---|---|---|---|---|
| $E_1$ | $E_2$ | $G_{12}$ | $\nu_{12}$ | $\nu_{23}$ |
| 131.0 | 13.0 | 6.4 | 0.34 | 0.35 |

[a]T300/5208 (NARMCO), fiber volume fraction is 0.63.
[b]The subscripts 1, 2, and 3 correspond to the longitudinal, transverse, and thickness directions, respectively, of a unidirectional ply.

cyclic loads were applied at a stress ratio of 0.1. The debond initiated at the lap end. Subsequent cyclic debonding was monitored throughout each test.

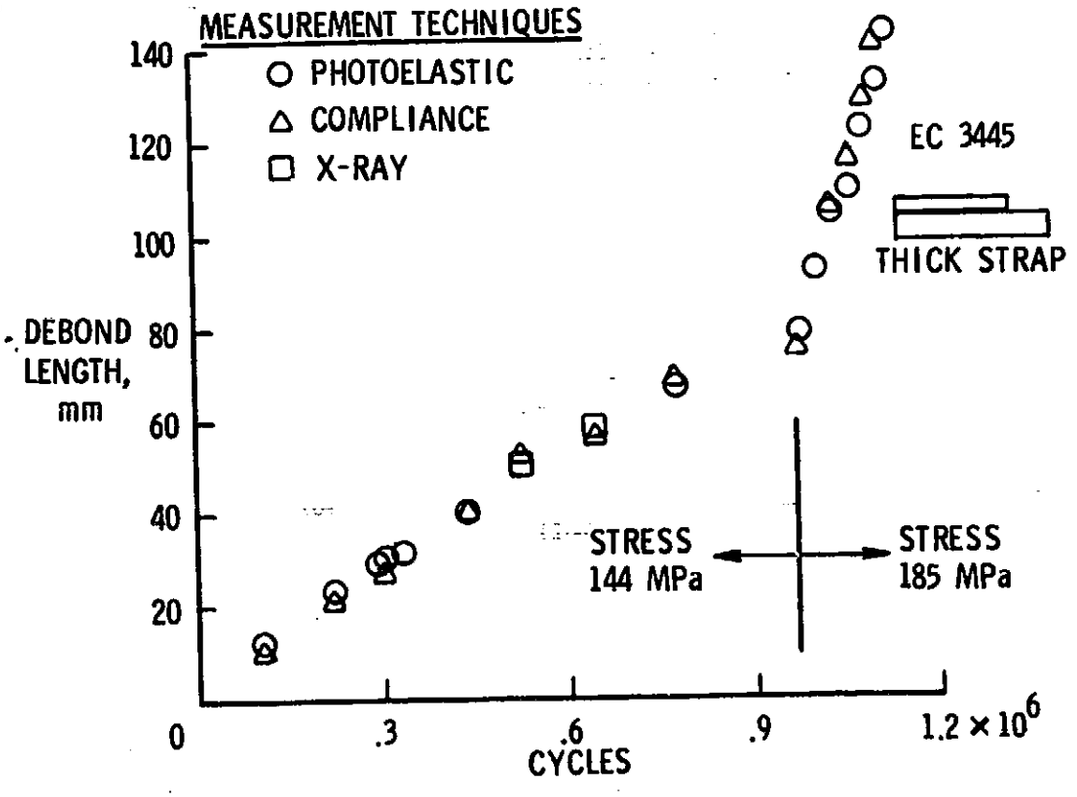


Figure 2. Comparison of different techniques to measure debond growth.

Three techniques to measure the cyclic debond growth were evaluated. For each technique, the location of the debond front was measured periodically to calculate debond growth rates. The first method used a sheet of photoelastic material bonded to the lap adherend of the specimen, as discussed in reference 4. Isochromatic fringes developed at the debond front as a result of the high strain gradient in that vicinity when subjected to load. These isochromatic fringes were observed through a polarizer and were used to locate the debond front. The second method involved locating the debond front with an X-ray technique using a dye penetrant zinc iodine. The third method involved measuring the compliance of the specimen and then calculating the debond length using a crack length compliance formula. The compliance of the specimen was measured with two displacement transducers attached on opposite sides of the specimen. All three methods provided good agreement for debond growth measurement as shown in Figure 2. In the present study the photoelastic technique was selected; an automated measurement system photographed the isochromatic fringes at predetermined intervals.

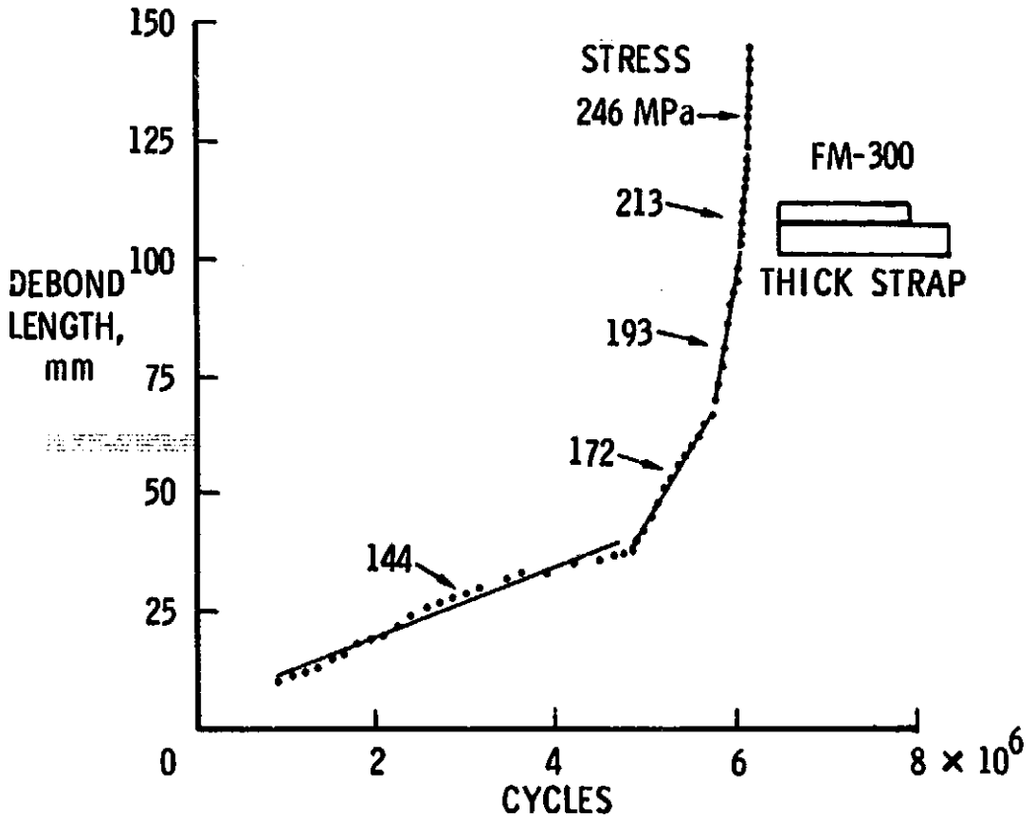


Figure 3. Typical variation of debond length with fatigue cycles at different stress levels.

The strain energy release rates ($G_T$, $G_I$, and $G_{II}$) are usually uniform in the cracked-lap-shear specimen for a significant debond growth region.[8] The debond data were measured over this region. This region is discussed in the subsequent section on finite-element analyses. Tests were conducted at two or more constant amplitude stress levels to get several values of debond growth rate (da/dN) from each specimen. At each stress level, the debond was measured as it grew over about 3 to 4 cm to ensure an accurate estimate of the debond growth rate over that region. Figure 3 shows typical debond data for different stress levels. In all cases debonding was initially nonlinear, but became linear after the debond progressed a short distance (about 10 mm). For each stress level, the debond data were fitted with a straight line using regression analysis.

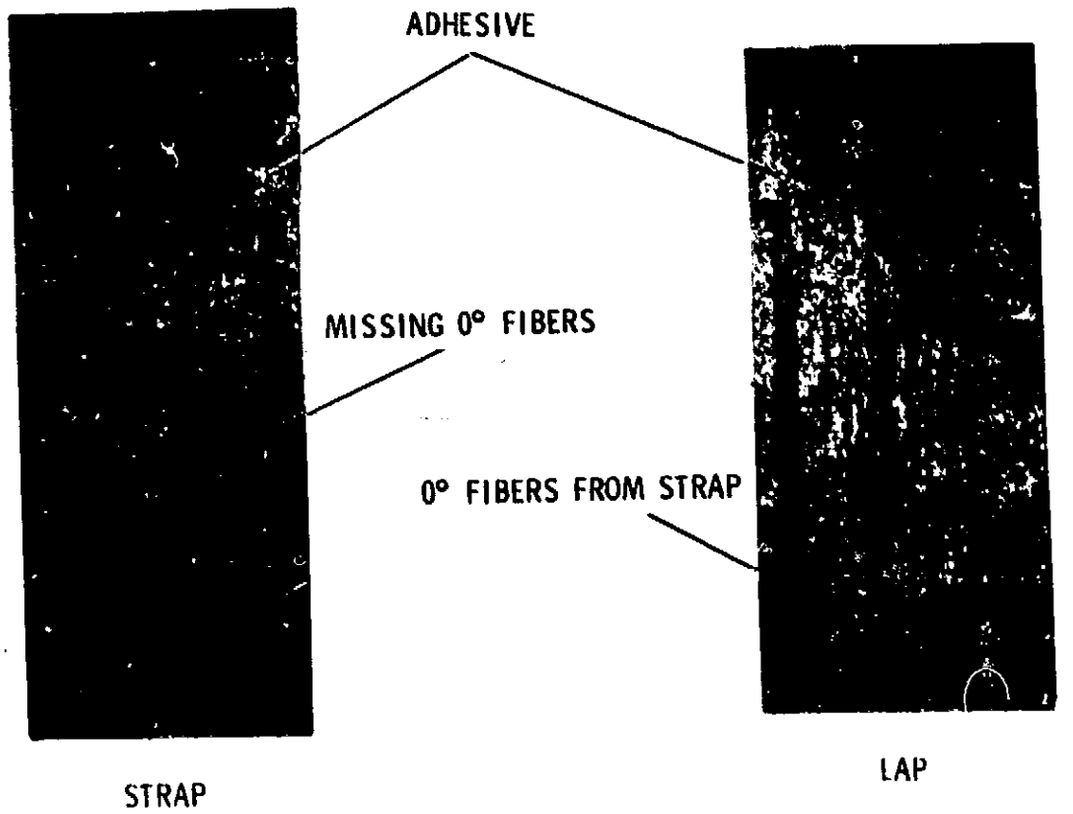


Figure 4. Debonded surfaces of cracked-lap-shear specimen (EC 3445, thick strap).

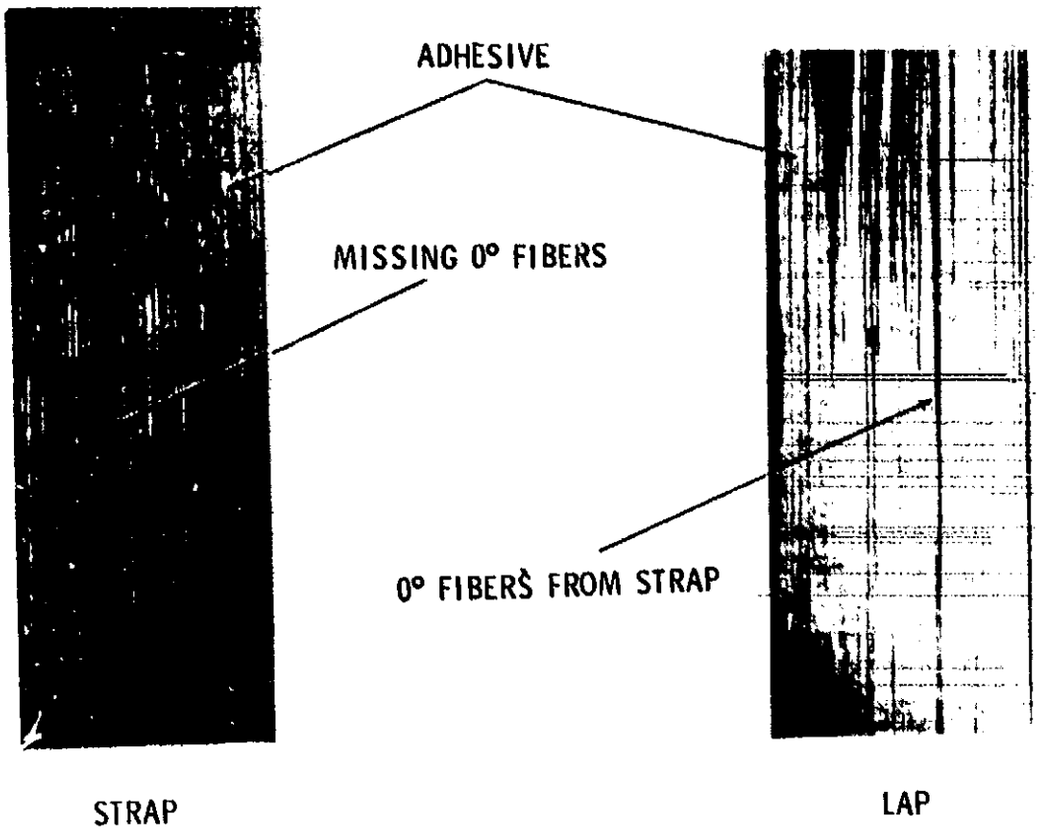


Figure 5. Debonded surfaces of cracked-lap-shear specimen (FM-300, thin strap).

## Debond Surfaces

As previously mentioned, the possible failure modes in a composite bonded joint are cyclic debonding, delamination, adherend fatigue, or a combination of these. All specimens in the present study failed primarily by cyclic debonding of the adhesive. Although some adhesive remained on both the strap and lap adherends, significantly more adhesive remained on the lap adherend. Also, there was some $0^{\circ}$ fiber pull-off from the strap adherend in most specimens. Typical debonded surfaces with these failure details are shown in Figures 4 and 5 for both systems. On close examination of the debonded surface, the following conclusions regarding the cyclic debond can be drawn. The debond was basically of a cohesive nature, i.e., failure was within the adhesive with some $0^{\circ}$ fiber pull-off from the strap. Further, the debond was always closer to the strap than to the lap. A possible explanation for this debond characteristic is discussed in the next section.

## FINITE-ELEMENT ANALYSIS

Previous studies of fatigue damage mechanisms in adhesively bonded joints have shown that the strain energy release rate, defined from fracture mechanics principles, may be useful for correlating cyclic debond growth rate.[4,5] Therefore, all four sets of specimens were analyzed with a finite element program, called GAMNAS[8] to calculate strain energy release rates. This two-dimensional analysis accounted for the geometric nonlinearity associated with the large rotations in the unsymmetric cracked-lap-shear specimen. The importance of a geometric nonlinear analysis for the cracked-lap-shear specimen has been discussed in detail in reference 8.

A typical finite-element mesh, shown in Figure 6, consisted of about 1600 isoparametric four-node elements and had about 3000 degrees of freedom. Each ply of composite was modeled as one layer in the finite-element model, except for the ply at the adhesive interface which was modeled in two or three layers. A multipoint constraint was applied to prevent rotation of the loaded end of the

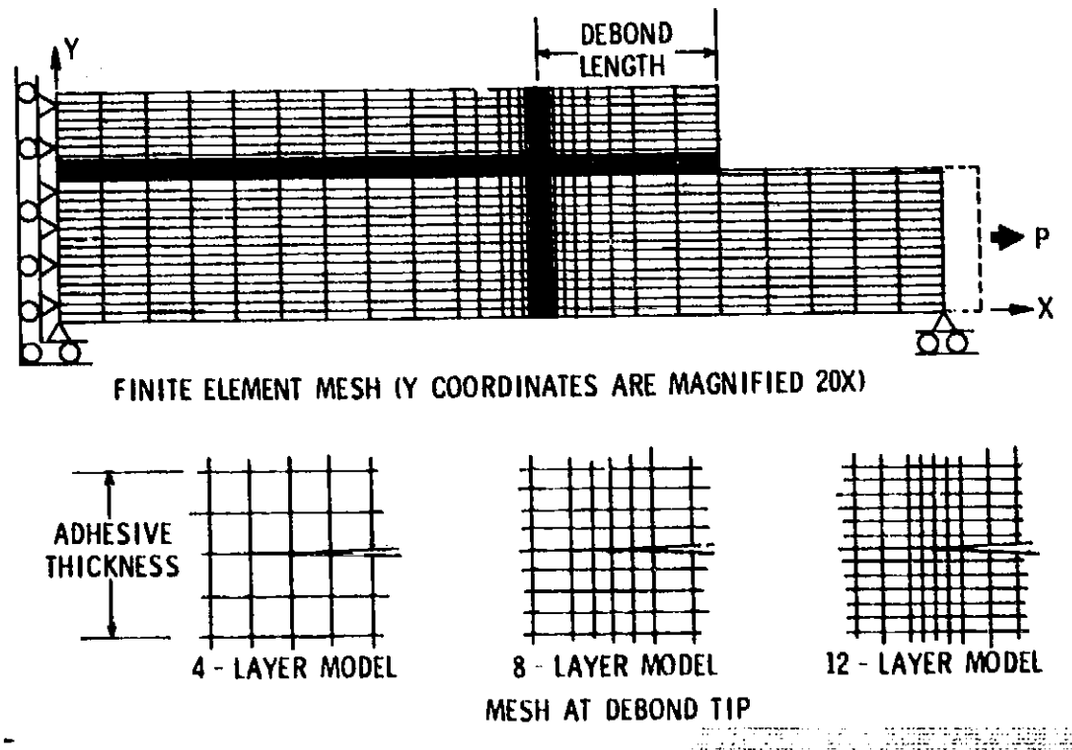


Figure 6. Finite element model.

model (i.e., all the axial displacements along the ends are equal) to simulate actual grip loading of the specimen. A double-cracked-lap-shear specimen with isotropic adherends was analyzed using a quasi-three-dimensional analysis like that in reference 13 to show that the present two-dimensional analysis should be based on the plane strain condition. The strain energy release rates $G_T$, $G_I$, and $G_{II}$ in the analysis were computed for the maximum load in the fatigue cycle using a virtual crack closure technique.[14] The details of this procedure are given in reference 8. The calculation of strain energy rates in the present analysis depends on three parameters: (1) debond location, (2) load level, and (3) debond length. These parameters will be discussed next.

As mentioned previously, the debond grew near the interface of the adhesive and strap adherend in all tests. It was very difficult to measure the exact location of the debond, but in general the debond grew within one-fourth of the thickness of adhesive closest to interface. The effect of the location of the debond within the adhesive in the cracked-lap-shear specimen was investigated using GAMNAS.[8] Figure 7 shows the variation of calculated $G_T$, $G_I$, and $G_{II}$ with the debond location within the thickness of the EC 3445 adhesive. These results were calculated by modeling the adhesive

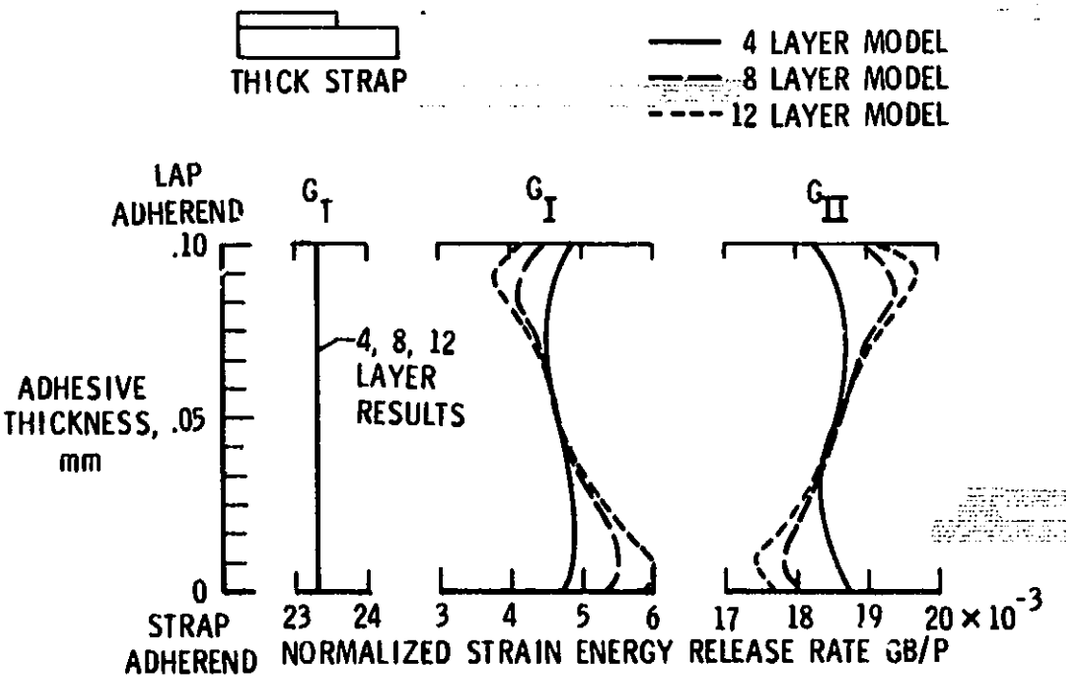


Figure 7. Variation of strain energy release rate with location of debond within EC 3445 adhesive.

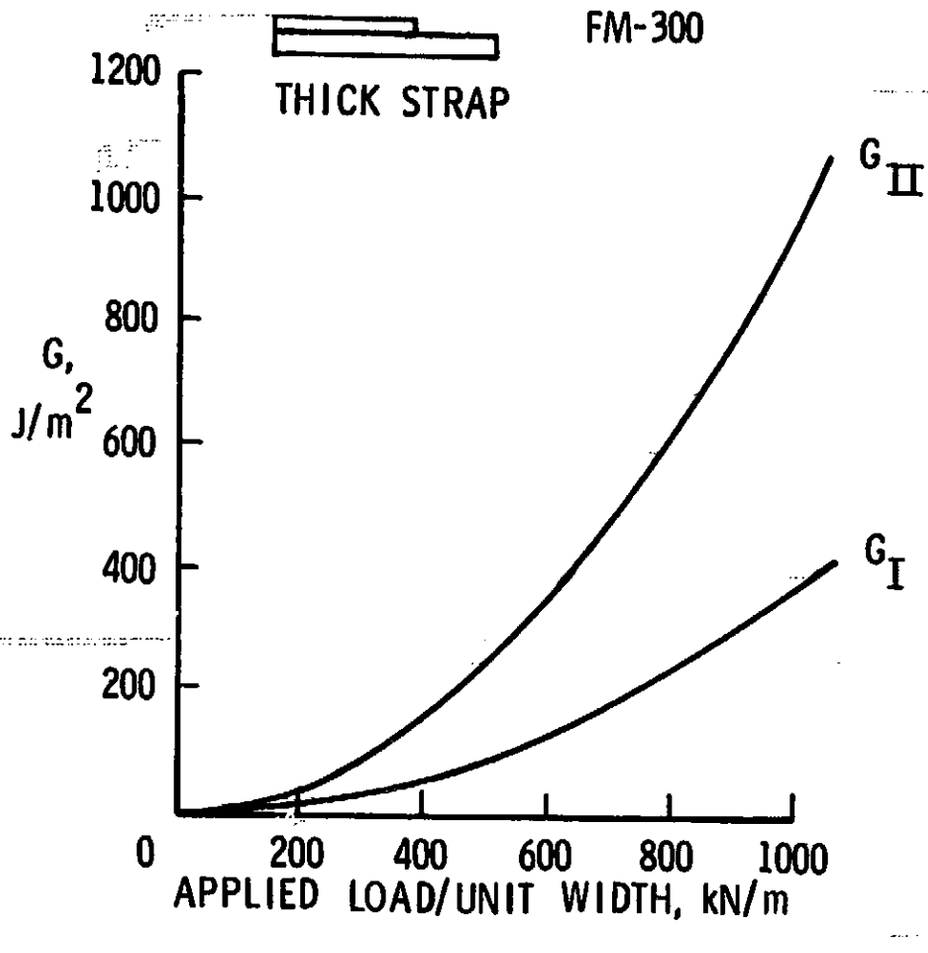


**Figure 8. Variation of strain energy release rates with applied load.**

with 4, 8, and 12 layers of elements, as shown in figure 6. Figure 7 clearly shows that $G_T$ remains constant for all locations of the debond, while $G_I$ has its maximum value near the adhesive-strap interface and $G_{II}$ has its maximum value near the adhesive-lap interface. The debond always initiated and grew in the region of highest $G_I$ (near the adhesive-strap interface). This indicates that $G_I$ has the greater influence on the debond location in the adhesive joint. This is consistent with the observations that adhesives are inherently weaker under peel loading than under shear loading.[1,2,15] Additionally, these results show that an accurate evaluation of $G_T$ can be achieved by a four layer model, while accurate evaluation of $G_I$ and $G_{II}$ requires a more refined model. To

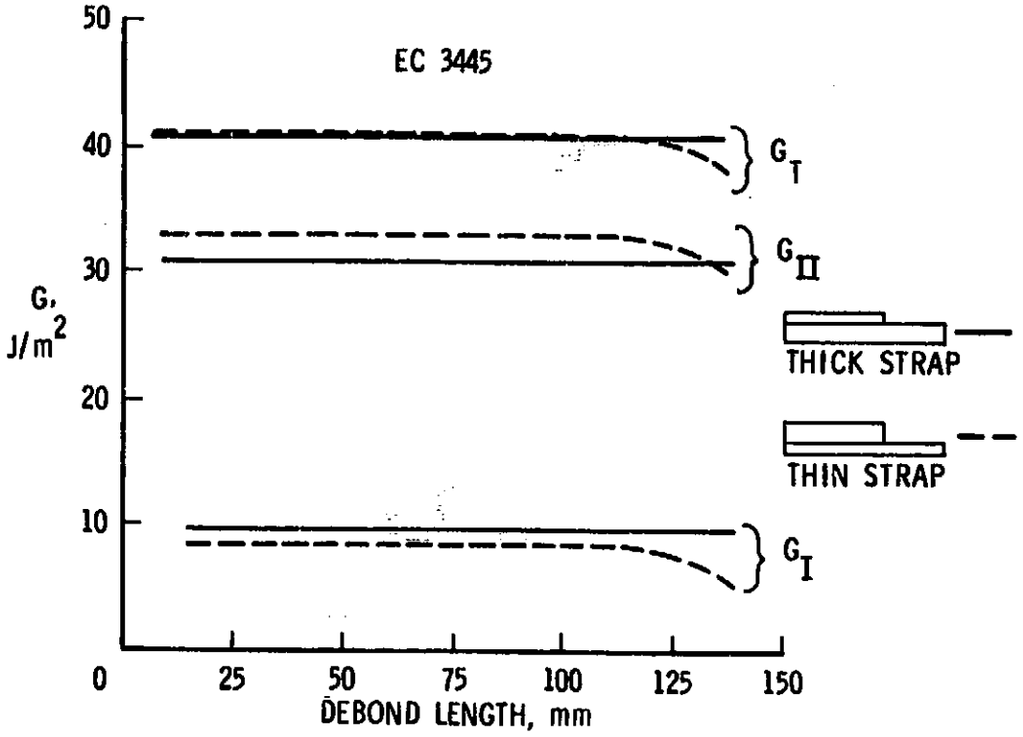


Figure 9. Variation of strain energy release rates with debond length.

analyze the experimental debond growth rates, the debond location for all subsequent calculations was selected by engineering judgement to be at one-sixth of the adhesive thickness away from the adhesive-strap interface. Also, the 12-layer model was used in these calculations.

Figure 8 shows the typical variation of strain energy release rates $G_I$ and $G_{II}$ with the applied load on the cracked-lap-shear specimen obtained from geometric nonlinear analyses. The $G_I$ and $G_{II}$ in nonlinear analysis were found to be functions of the square of applied load within one percent.

All four sets of specimens were then analyzed to determine the variation of $G_T$, $G_I$, and $G_{II}$ with the debond length. Figure 9 shows the typical dependence of $G_T$, $G_I$, and $G_{II}$ on the debond length for both types of specimen with EC 3445 adhesive. For specimens with thick straps, $G_T$, $G_I$, and $G_{II}$ were constant up to 140 mm of debond length. Similar behavior was found for co-cured specimens with thick straps. For specimens with thin straps,

Table III. Strain Energy Release Rate

| Specimen Details | | Strain Energy Release Rate[a] ($J/m^2$) for the Applied Stress of 82.0 MPa | | |
|---|---|---|---|---|
| Adhesive | Strap Type | $G_I$ | $G_{II}$ | $G_I/G_{II}$ |
| EC 3445 (Secondary bonding) | Thick | 9.75 | 31.08 | 0.31 |
| | Thin | 8.23 | 33.20 | 0.25 |
| FM-300 (Co-cure bonding) | Thick | 11.21 | 29.60 | 0.38 |
| | Thin | 10.66 | 32.40 | 0.33 |

[a]Calculated with debond location at one-sixth of adhesive thickness from the strap-adhesive interface.

$G_T$, $G_I$, and $G_{II}$ were constant up to debond lengths of 115 mm and 65 mm in secondary and co-cure bonded systems, respectively. The constant values of strain energy release rates for all four sets of specimens are provided in Table III for a specified stress level.

## RESULTS AND DISCUSSIONS

An attempt was made to determine if one of the components of strain energy release rate ($G_T$, $G_I$, or $G_{II}$) dominates the cyclic debonding. The measured debond growth rates were, therefore, correlated with each of the calculated strain energy release rates $G_I$, $G_{II}$, and $G_T$. These correlations are shown in Figures 10 and 11 for EC 3445 and FM-300, respectively. If one component of strain energy release rate had a dominant influence, it would correlate significantly better than the others when debond data from specimens with different $G_I$-to-$G_{II}$ ration are compared.

An equation of the form

$$\frac{da}{dN} = c(G)^n \qquad (1)$$

was fitted to the data in Figures 10 and 11 by using a least-squares regression analysis. The values of $c$ and $n$, as well as the sum of errors, $\Sigma r^2$, are shown in the figures. For each adhesive, the values of $\Sigma r^2$ are about the same for the $G_I$, $G_{II}$, and $G_T$. However, the $\Sigma r^2$ term is lowest for $G_T$, indicating that $G_T$ provided a somewhat better correlation than either $G_I$ or $G_{II}$. This suggests that debond growth rate is a function of the combined

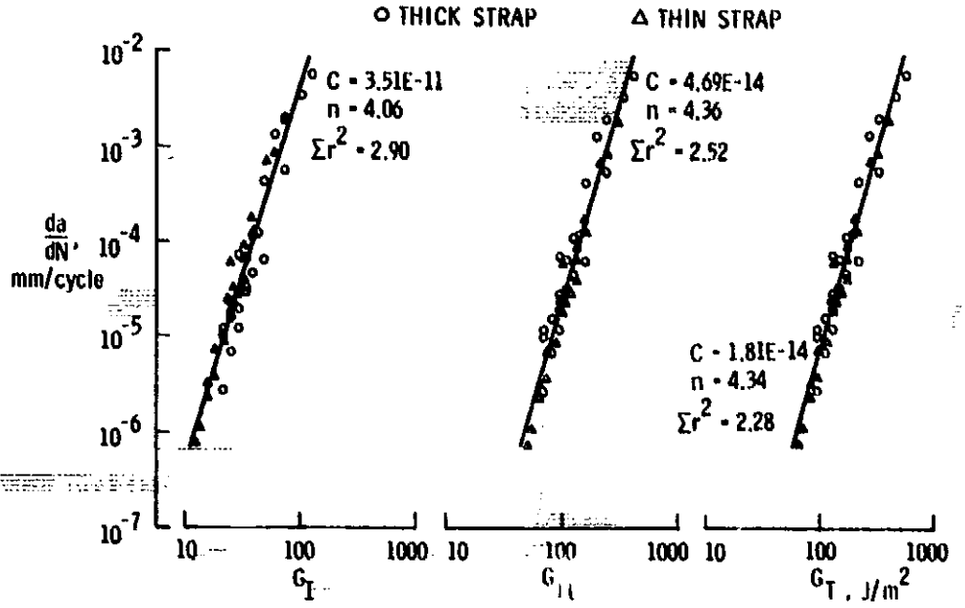


Figure 10. Relation between strain energy release rates and debond growth rate for EC 3445 adhesive.

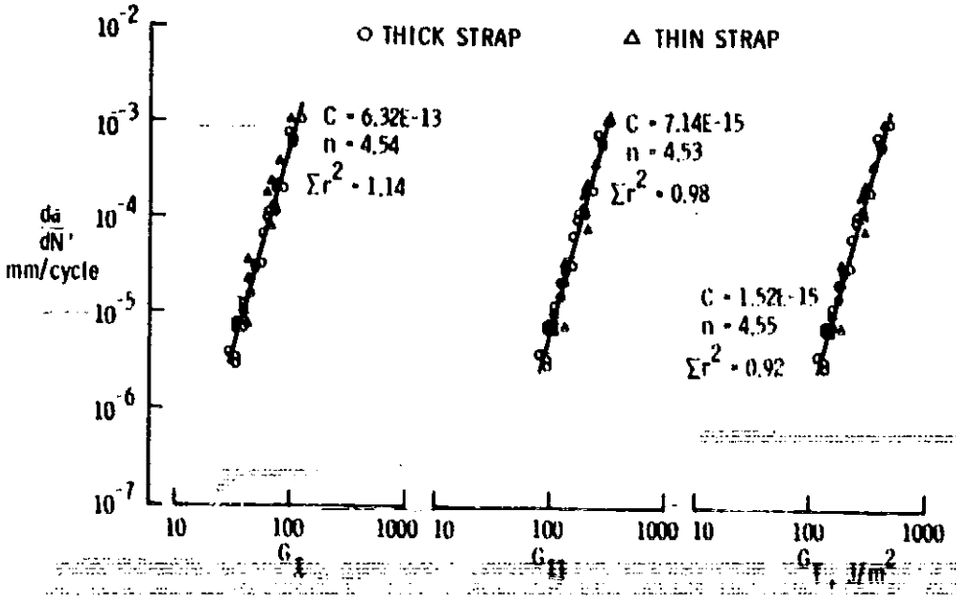


Figure 11. Relation between strain energy release rates and debond growth rate for FM-300 adhesive.

effects of $G_I$ and $G_{II}$. However, the $G_I$-to-$G_{II}$ ratios for the test specimens were all within the rather narrow range of 0.25 to 0.38. As a result, it is not surprising that $G_I$, $G_{II}$, and $G_T$ all did a reasonably good job of correlating the data in Figures 10 and 11. Furthermore, each figure shows that data from both specimen geometries are within an acceptable scatter band (similar to that observed in fatigue crack propagation in metals).[16] This indicates that specimen geometry did not influence the relationship between the debond growth rate and strain energy release rate. The relations between da/dN and $G_T$, for both adhesives, are compared in Figure 12. This figure shows that the debond rate with FM-300 is about 40 percent of that for EC 3445 for the same applied load and debond length.

Because of the log-log scale in Figure 12, the curves relating da/dN and G have slopes equal to the n term in Equation (1). The values of n found in this investigation ranged from 4 to 4.5. This is quite high compared to typical values of n for fatigue crack growth in aluminum and steel alloys that range from 1.5 to 3.[16] These steep slopes mean that a small change in applied load would cause a large change in debond growth rate. Thus, the debond propagation in adhesive joints is more sensitive to errors in design loads than are typical cracks in metallic structures. Because of these steep slopes, it may be difficult to design bonded joints for finite life. Minor design alterations or small analysis errors could cause a much shorter life than the design value.. A viable alternative would involve an infinite-life approach. For this purpose, the no-growth threshold, $G_{th}$, (based on $G_T$ for discussion purpose here) may be an important material property for bonded systems. If a $10^{-6}$ mm/cycle rate is arbitrarily assumed to be the no-growth threshold, the curves in Figure 12 show that $G_{th}$ values for EC 3445 and FM-300 are 60.8 J/m$^2$ and 90.5 J/m$^2$, respectively. These $G_{th}$ values are equivalent to applied stresses (based on nominal area of strap) of 100 MPa and 121 MPa for EC 3445 and FM-300, respectively.

The threshold strain energy release rate, $G_{th}$, appears to depend on the adhesive and not on the specimen geometry within the range of this study. As a result, a $G_{th}$ value and an analytical method such as GAMNAS[8] could be employed during design to determine the maximum cyclic loads to obtain an infinite fatigue life for bonded structural components. An initial debond must be assumed to exist in order to calculate strain energy release rate. The size of the initial debond can be estimated from the anticipated manufacturing defects or NDI limitations. The maximum design load can then be determined to ensure that the applied $G_T$ in the bondline is below $G_{th}$ for the given adhesive. In the present study the values of $G_{th}$ for EC 3445 and FM-300 were obtained under laboratory ambient conditions. However, as with other adhesive properties, it is anticipated that $G_{th}$ will be influenced by the

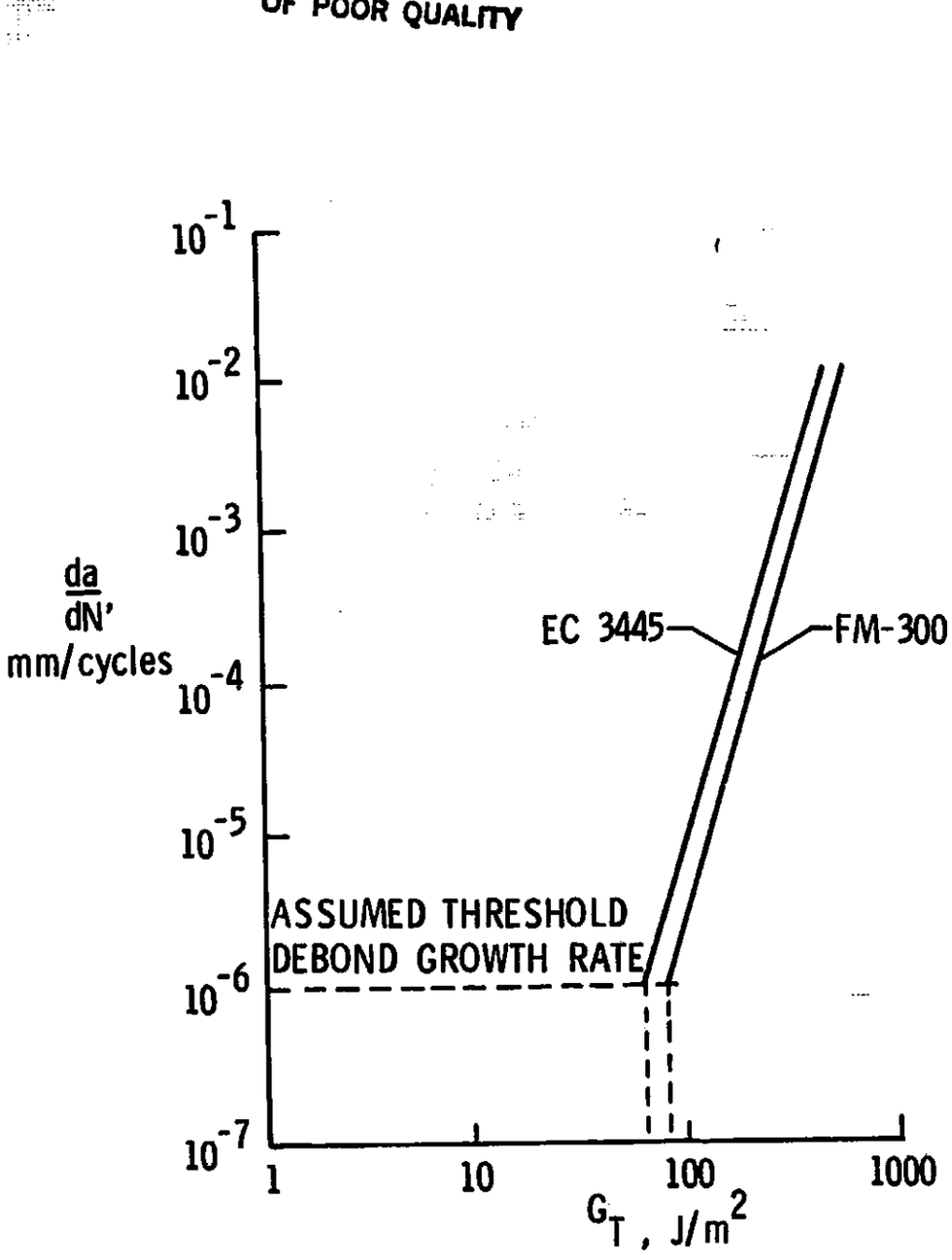


Figure 12. Comparison of debond growth rate between two adhesives.

environmental conditions. Perhaps, the present procedures can be extended to account for such environmental effects.

## CONCLUSIONS

A combined experimental and analytical study of the cracked-lap-shear specimen subjected to constant-amplitude cyclic loading

was undertaken to analyze the fatigue behavior of simple composite-to-composite bonded joints. Two bonded systems were studied—graphite/epoxy adherends bonded with EC 3445 adhesive in a secondary bonding procedure and with FM-300 adhesive in a co-cure bonding procedure. With each bonded system, two specimen types were tested: (1) strap adherend of 16 plies bonded to lap adherend of 8 plies, and (2) strap adherend of 8 plies bonded to lap adherend of 16 plies. A finite-element analysis was conducted to calculate the strain energy release rates: $G_I$ due to peel stress, $G_{II}$ due to shear stress, and $G_T$ due to both stresses. The present study led to the following conclusions:

1. Cracked-lap-shear specimens were found to provide consistent debond growth data. The cyclic debond growth rates were reproducible from one specimen to another within a scatter band comparable to that for crack growth in metals.

2. Cracked-lap-shear specimens failed predominately by cyclic debonding of adhesive, accompanied by some $0^o$ fiber pull-off from the strap adherend.

3. The debond always grew in the region of the adhesive that had the highest mode I loading (peel stress or $G_I$). This indicates that $G_I$ had a stronger influence than $G_{II}$ on the debond location.

4. Debond growth rates correlated very well with $G_I$, $G_{II}$, and $G_T$. However, the specimen geometries tested in this study did not produce a wide enough range of mixed mode loading conditions to clearly establish the relative influences of strain energy release rates $G_I$, $G_{II}$, and $G_T$ on debond growth rate.

## ACKNOWLEDGMENTS

The first author is grateful for the support from the Army Structures Laboratory (RTL-AVRADCOM) through the In-house Laboratory Independent Research (ILIR) program during the course of this study.

## REFERENCES

1. F. L. Matthews, P. F. Kilty, and E. W. Godwin, "A Review of the Strength of Joints in Fibre-Reinforced Plastics, Part 2--Adhesively Bonded Joints," Composites, 13 (1), 29 (1982).
2. L. J. Hart-Smith, "Analysis and Design of Advanced Composite Bonded Joints," NASA CR-2218, National Aeronautics and Space Administration (1974).

3. W. J. Renton and J. R. Vinson, "The Analysis and Design of Composite Material Bonded Joints Under Static and Fatigue Loadings," AFOSR-TR-72-1627, U.S. Air Force (1973).
4. G. L. Roderick, R. A. Everett, Jr., and J. H. Crews, Jr., in "Fatigue of Composite Materials," ASTM STP 569, pp. 295-306, American Society for Testing and Materials, Philadelphia, 1975.
5. T. R. Brussat, S. T. Chiu, and S. Mostovoy, "Fracture Mechanics for Structural Adhesive Bonds," AFML-TR-163, Air Force Materials Laboratory (1977).
6. J. Romanko and W. G. Knauss, "Fatigue Behavior of Adhesively Bonded Joints," Vol. I, AFWAL-TR-80-4037, U.S. Air Force (1980).
7. R. A. Everett, Jr., "The Role of Peel Stresses in Cyclic Debonding," NASA TM-84504, National Aeronautics and Space Administration (1982).
8. B. Dattaguru, R. A. Everett, Jr., J. D. Whitcomb, and W. S. Johnson, "Geometrically-Nonlinear Analysis of Adhesively Bonded Joints," NASA TM-84562, National Aeronautics and Space Administration (1982).
9. G. R. Alsmiller, Jr. and W. P. Anderson, "Advanced Composites Airframe Program - Preliminary Design," USAAVRADCOM-TR-80-D-37A, U.S. Army (1982).
10. E. J. Hughes and J. L. Rutherford, "Evaluation of Adhesives for Fuselage Bonding," Report No. KD-75-74, The Singer Company (1975).
11. K. N. Shivakumar and J. H. Crews, Jr., "Bolt Clampup Relaxation in a Graphite/Epoxy Laminate," NASA TM-83268, National Aeronautics and Space Administration (1982).
12. L. J. Hart-Smith, "Effect of Adhesive Layer Edge Thickness on Strength of Adhesive-Bonded Joints," MDC J4675, McDonnell-Douglas Corporation (1981).
13. I. S. Raju and J. H. Crews, Jr., "Interlaminar Stress Singularities at a Straight Edge in Composite Laminates," Computers and Structures, 14 (1-2), 21 (1981).
14. E. F. Rybicki and M. F. Kanninen, "A Finite Element Calculation of Stress Intensity Factors by a Modified Crack Closure Integral," Engineering Fracture Mechanics, 9 (4), 931 (1977).
15. F. A. Keimel, in "Kirk-Othmer: Encyclopedia of Chemical Technology," Vol. 1, 3rd ed., pp. 488-510, John Wiley & Sons, New York, 1978.
16. "Damage Tolerant Design Handbook," Battelle Metals and Ceramics Information Center, Columbus, 1972.